JOURNAL OF THERMOPHYSICS AND HEAT TRANSFER
Vol. 17, No. 3, July–September 2003

Technical Notes

TECHNICAL NOTES are short manuscripts describing new developments or important results of a preliminary nature. These Notes cannot exceed six manuscript pages and three figures; a page of text may be substituted for a figure and vice versa. After informal review by the editors, they may be published within a few months of the date of receipt. Style requirements are the same as for regular contributions (see inside back cover).

High-Temperature, Nonreacting Flowfields Generated by a Hypersonic Chemical-Laser Nozzle

Eric L. Petersen,* Matthew J. A. Rickard,†
and Richard P. Welle‡
The Aerospace Corporation,
El Segundo, California 90245-4691

Nomenclature

M = Mach number of primary nozzle flow
P_b = backpressure outside nozzle
P_e = nozzle exit static pressure
u_e = exit velocity of primary nozzle fluid
u_j = velocity of secondary jet fluid
ρ_e = exit density of primary nozzle fluid
ρ_j = density of secondary jet fluid

Introduction

SINCE the first demonstration of continuous wave (cw) lasing from a HF chemical laser by Spencer et al.,[1] the gasdynamic flowfield of the laser gain zone has been the subject of much research. In a typical HF (or DF) laser, fluorine atoms are mixed with hydrogen (or dueterium) molecules to produce vibrationally excited HF* via the reaction $F + H_2 = HF^* + H$ (or $F + D_2 = DF^* + D$) (Ref. 1). The resulting low-pressure (1–20 torr) flowfield is very viscous, and in general, the mixing occurs mostly through transverse diffusion between reactant streams.[2,3] Ejecting the fluorine atoms through a bank of multiple hypersonic nozzles enhances the mixing process, and various methods have been utilized to produce the F-atom mixture, which typically has a stagnation temperature and pressure on the order of 1400–1800 K and 1–10 atm (Ref. 4). For the nozzle of interest herein, the H_2 is injected at an angle to the primary nozzle flow. This transverse injection is thought to stretch the reactant interface by increasing the strain rate between streams.[5]

HF and DF lasers are currently under consideration for use in a space-based laser system,[6] and there is renewed interest in further characterizing and improving the performance of the next generation of chemical lasers. With these applications in mind, the authors set up a shock tube and optical imaging technique to study the flowfields of chemical laser nozzles. However, the present work differs from previous chemical-laser shock-tube experiments[7] because the shock tube was utilized more as a shock tunnel to study the details of the mixing and reaction phenomena instead of producing actual laser gain. This Note describes the shock-tunnel facility and presents schlieren images from a nonreacting, single-nozzle flowfield.

Experiment

For the present study, The Aerospace Corporation shock tube, primarily employed for reflected shock chemistry experiments,[8] was mated to a test section and a large dump tank (Fig. 1). Supersonic flowfield experiments can be performed in the test section under vacuum conditions by mounting a nozzle, such as a full-scale chemical laser nozzle, in the endwall. The gas between the reflected shock wave and the endwall simulates the high-temperature stagnation conditions upstream of a chemical-laser nozzle.

Figure 1 presents a schematic view of the shock-tube facility and diagnostics. The pressure-driven shock tube has a 3.5-m driver with a 7.62-cm internal diameter. The driven section is approximately 11 m long with a 16.2-cm internal diameter. Single, pre-scribed aluminum diaphragms (2–3 mm thick) were utilized in the present experiments; helium served as the driver gas, and research-grade N_2 was employed as the driven gas.

Incident-shock velocities were detected using three fast-response (1 μs), PCB 113A piezoelectric pressure transducers and two Fluke PM6666 time-interval counters. The velocity-detection transducers were amplified to increase their sensitivity to the step increase in pressure upon arrival of the incident shock wave. A fourth transducer, located 5 cm upstream of the nozzle supply cavity, monitored the stagnation pressure conditions behind the reflected shock wave. The temperature and pressure behind the reflected shock were calculated using the measured shock velocity in the usual manner.

Located at the endwall of the shock tube was the nozzle with characteristics similar to a chemical-laser nozzle. A view of the two-dimensional, annodized aluminum nozzle is presented in Fig. 2. The nozzle was separated from the shock tube by a lightly scribed, 0.15-mm aluminum diaphragm that ruptured on reflection of the shock wave from the endwall. The straight-walled nozzle had a 0.41-mm throat gap, a 10.16-mm exit height, and a 15-deg expansion half-angle. These dimensions correspond to an average exit Mach number of 5.0 for a specific heat ratio of 1.4. Near the top and bottom

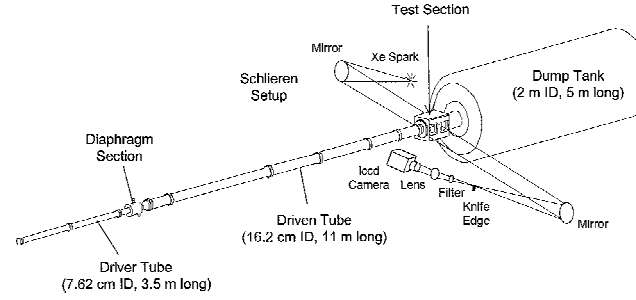

Fig. 1 Shock-tunnel facility and conventional schlieren diagnostic. He driver gas and N_2 test gas; xenon flashlamp with a 10-μs pulse provides light source for schlieren setup.

Received 16 September 2002; revision received 14 October 2002; accepted for publication 14 October 2002.

*Senior Member of the Technical Staff, Space Materials Laboratory; currently Assistant Professor, Mechanical, Materials and Aerospace Engineering, University of Central Florida, P.O. Box 162450, Orlando, FL 32816. Member AIAA.

†Member of the Technical Staff, Space Materials Laboratory; currently Ph.D. Student, Mechanical and Aerospace Engineering, 4200 Engineering Gateway, University of California Irvine, Irvine, CA, 92612.

‡Project Leader, Space Materials Laboratory, Mail Stop M5-753, 2350 East El Segundo Boulevard, Member AIAA.

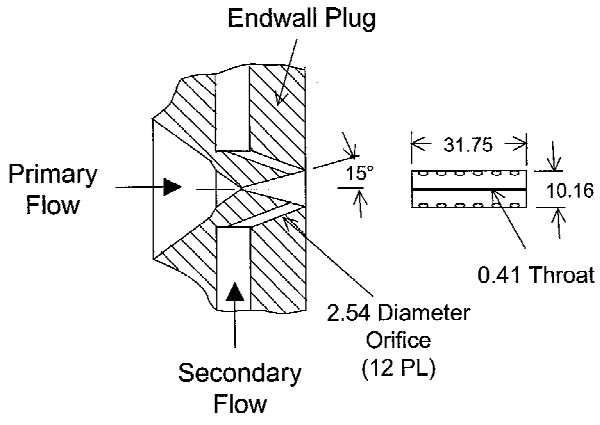

Fig. 2 Model chemical-laser nozzle used in the experiments: all dimensions in millimeters, and the corresponding exit Mach number is 5.

lips of the nozzle were two rows of six, 2.54-mm-diam secondary injection holes spaced 5.1 mm apart. These orifices were situated at a 35-deg angle relative to the nozzle wall and were connected to a supply cavity.

The nozzle gases exhausted into a 25-cm-square test section with glass windows for optical access. A constant vacuum pressure was maintained in the test section by a 2-m-diam, 15-m^3 dump tank. The dump tank is connected to a large-capacity roughing- and diffusion-pump system and has a combined leak and outgassing rate less than 1 torr/h. The present experiments employed the roughing pump alone because only backpressures between approximately 25 and 100 torr were needed.

The schlieren diagnostic consisted of a xenon flashlamp (EG&G MVS-2601) with a 10-μs pulse width and two, 26.7-cm-diam parabolic mirrors with a focal length of 1.534 m. The light was focused onto a horizontal knife edge and collimated by a 2.54-cm-diam lens with an f-number of 11.8 onto a Princeton Instruments intensified charge-coupled device (ICCD-576S/RB) camera driven by a ST-130 controller and a PG-200 pulser. A narrowband filter centered at 470 nm prevented background emission from reaching the camera. The camera shuttering and image processing were performed using the Princeton Intruments WinView software, version 1.3B. For each experiment, the reflected-shock pressure 5 cm upstream of the nozzle entrance plane, the flashlamp signal, the CCD intensifier gate, and the trigger signal were monitored using a high-speed, 16-bit computer-based oscilloscope from Gage Applied Sciences (Compuscope 512).

Procedure

Most experiments were performed with an average reflected shock temperature of 1770 K and a pressure of 18 atm. On some experiments, nozzle stagnation conditions as low as 1380 K and as high as 26 atm were realized. The shocked gas behind the reflected wave maintained steady conditions for approximately 2 ms, and the corresponding time for steady flow in the nozzle began approximately 0.5 ms after shock reflection and lasted for at least 1 ms.

Within approximately 1 min of bursting the primary diaphragm, the airflow to the secondary injection orifices was initiated manually to ensure steady flow at the time of arrival of the primary-nozzle gas. During this time, the large dump-tank volume assured the test-section pressure did not increase more than a fraction of a torr above the initial back pressure. Timing of the flashlamp spark and intensifier gate was performed using the signal from a velocity-detection transducer as a trigger. This trigger signal was sent to a programmable pulse generator (BNC Model 500) with an internal delay time defined such that the subsequent pulse sent to the camera and flashlamp occurred at a repeatable time during steady nozzle flow, approximately 1 ms after arrival of the reflected shock wave. The intensifier of the CCD camera was gated for 20 μs.

For each experiment, the sonic secondary air jets were supplied with a 5.1-atm pressure at 295 K. The resulting mass flow per unit area was 0.036 kg/$cm^2 \cdot$ s. This flow rate can be compared to the nominal nozzle mass flux of 0.17 kg/$cm^2 \cdot$ s (1780-K, 18-atm stagnation conditions). A useful parameter for characterizing jets in a supersonic crossflow is the momentum flux ratio, that is, $(\rho u^2)_j/(\rho u^2)_\infty$. The nominal ratio was 3.2 for the present case.

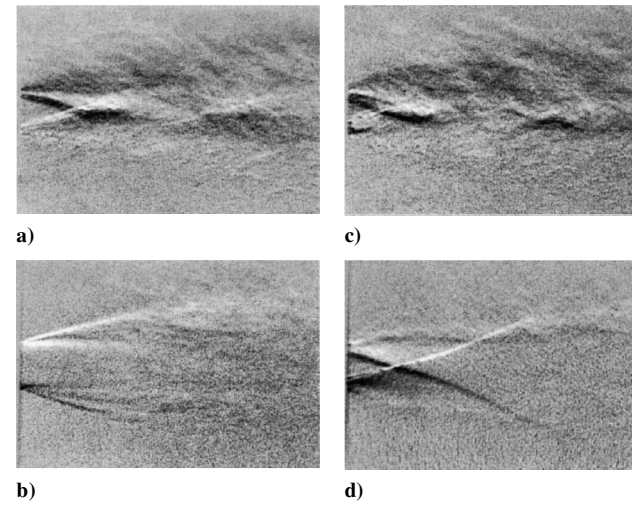

Fig. 3 Schlieren images of the nozzle flowfield with and without secondary jets: a) nozzle flow only, overexpanded (P_e/P_b = 0.26) primary nozzle flow, 1770 K, 18 atm, and P_b = 100 torr; b) nozzle flow only, slightly underexpanded (P_e/P_b = 1.3) primary nozzle flow, 1380 K, 22 atm, and P_b = 30 torr; c) combined jet and nozzle flow, overexpanded (P_e/P_b = 0.26) primary nozzle flow, 1770 K, 18 atm, and P_b = 100 torr; and d) combined jet and nozzle flow, slightly underexpanded (P_e/P_b = 1.3) primary nozzle flow, 1520 K, 26 atm, and P_b = 25 torr.

Results

Representative schlieren images of the nozzle flowfield with and without secondary injection are presented in Figs. 3a–3d. In figs 3a and 3b, the image is from the hypersonic primary nozzle without secondary injection, and the Figs. 3c and 3d image is from the primary nozzle flow with secondary injection.

Figures 3a and 3c were taken from a set of experiments wherein the primary nozzle flow was overexpanded with a nominal exit-to-back static pressure ratio (P_e/P_b) of 0.26. The stagnation conditions were 1770 K and 18 atm, and the corresponding backpressure was 100 torr. Strong compression waves due to the overexpansion are evident in Fig. 3a, and Fig. 3c indicates that the presence of the transverse jets near the nozzle exit further influences the flowfield and shock structure.

A slightly underexpanded case ($P_e/P_b = 1.3$) is shown in Figs. 3b and 3d, with and without the transverse jets. Figure 3b shows a rather clean central core due to the near-ideal expansion of the Mach 5 gas with a 1380-K, 22-atm supply exhausting into a 30-torr backpressure. However, the secondary jets have a significant effect on the structure of the nozzle flowfield, where a distinct shock structure is evident in the schlieren image [1520 K and 26 atm, (Fig. 3d)] when compared to the image with no secondary jet flow (Fig. 3b).

Conclusions

A shock-tube facility was modified to include a single endwall-mounted chemical-laser nozzle, a windowed test section simulating a constant-pressure laser cavity, and a 15-m^3 dump tank. Shock-heated N_2 (1380–1780 K and 17–26 atm) simulated the primary $M = 5.0$ nozzle flow, and air simulated the secondary-injection gas from a single row of sonic orifices. Single-frame schlieren images of the flowfield with and without secondary injection were obtained. The resulting images show shock-structure details that are useful in the understanding and optimization of chemical-laser nozzles.

References

[1] Spencer, D. J., Jacobs, T. A., Mirels, M., and Gross, R. W. F., "Continuous-Wave Chemical Laser," *International Journal of Chemical Kinetics*, Vol. 1, No. 5, 1969, pp. 493, 494.

[2]Broadwell, J. E., "Effect of Mixing Rate on HF Chemical Laser Performance," *Applied Optics*, Vol. 13, No. 4, 1974, pp. 962–967.
[3]Mirels, H., Hofland, R., and King, W. S., "Simplified Model of Continuous-Wave Diffusion-Type Chemical Laser," *AIAA Journal*, Vol. 11, No. 2, 1973, pp. 156–164.
[4]Gross, R. F. W., and Bott, J. F. (eds.), *Handbook of Chemical Lasers*, Wiley, New York, 1976.
[5]Driscoll, R. J., "Effect of Reactant-Surface Stretching on Chemical Laser Performance," *AIAA Journal*, Vol. 22, No. 1, 1984, pp. 65–74.
[6]Acebal, R., "Hydrogen Fluoride vs Deuterium Fluoride Space-Based Laser Performance Comparison," *AIAA Journal*, Vol. 36, No. 3, 1998, pp. 416–419.
[7]Rose, P. H., "Advanced Laser Technology Development in Shock Tubes," *Shock Tube and Shock Wave Research*, edited by B. Ahlborn, A. Hertzberg, and D. Russell, Univ. of Washington Press, Seattle, WA, 1978, pp. 508–518.
[8]Bott, J. F., and Cohen, N., "A Shock Tube Study of the Reaction of Methyl Radicals with Hydroxyl Radicals," *International Journal of Chemical Kinetics*," Vol. 23, No. 11, 1991, pp. 1017–1033.

Derivation of Heat-Flux Dependence on Pressure Gradient

Abdulmuhsen H. Ali*
Kuwait University, Safat 13060, Kuwait

Nomenclature

$E(\boldsymbol{r}, t)$	=	total energy
$f(\boldsymbol{r}, \boldsymbol{v}, t)$	=	local equilibrium Maxwellian
$\boldsymbol{J}_E(\boldsymbol{r}, t)$	=	average heat-flux vector
k_B	=	Boltzmann constant
$P^{(\bar{N})}$	=	$\bar{N}$ particle specific distibution function
$p(\boldsymbol{r}, t)$	=	pressure
$\boldsymbol{r}$	=	position vector
$T(\boldsymbol{r}, t)$	=	temperature
t	=	time
$\boldsymbol{v}$	=	microscopic velocity
$\triangle \boldsymbol{a}$	=	an element of area
$\rho(\boldsymbol{r}, t)$	=	mass density

Introduction

In the derivation of Cattaneo's heat-flux law that was presented before,[1–3] some steps were approximations, which were done for the purpose of demonstrating the salient feature of the heat-flux law that results from energy dynamics considerations. For example, the equalities $\langle E\boldsymbol{v}\rangle = \langle E\rangle\langle \boldsymbol{v}\rangle$ and $\langle Ev^2\rangle = \langle E\rangle\langle v^2\rangle$ were used, and the extra terms on the right-hand side of the preceding equalities were not included in the final result. Moreover, the distibution function needed to be the constant $[1-(8/3\pi)]$ multiplied by the local Maxwellian in order for the Eucken number to be close to the value 2.5, and the gas needed to have an overall speed that is higher than the sonic speed. The purpose of this Note is to show that when the extra terms are included then one would recover the preceding result with an additional term, which is the pressure gradient. Also, the consistancy of the energy equation presented before[1] with the the energy equation in transport phenomenon is explained here. It is shown that under certain conditions the heat-flux law will depend simultaneously on temperature and pressure gradients. The heat flow dependence on pressure gradient was suggested by Truesdell and Toupin and Champman and Cowling, as was discussed by Roetman.[4] This dependence helps deriving a hyperbolic heat equation, which is the needed equation for heat conduction with finite signal time.

Statistical Mechanical Derivation of the Pressure Gradient Term

To derive the constitutive heat-flux law, which includes the relaxation time from the principles of energy transport, one needs to consider the following relations:

$$\boldsymbol{J}_E(\boldsymbol{r}, t) = \frac{1}{2}\rho(\boldsymbol{r}, t)\langle v^2\boldsymbol{v}\rangle = \frac{1}{2}\rho(\boldsymbol{r}, t)\frac{\int d^3v f(\boldsymbol{r}, \boldsymbol{v}, t)v^2\boldsymbol{v}}{n(\boldsymbol{r}, t)} \quad (1)$$

$$\rho_E(\boldsymbol{r}, t) = \frac{1}{2}\rho(\boldsymbol{r}, t)\langle v^2\rangle = \frac{1}{2}\rho(\boldsymbol{r}, t)\frac{\int d^3v f(\boldsymbol{r}, \boldsymbol{v}, t)v^2}{n(\boldsymbol{r}, t)} \quad (2)$$

where $\rho(\boldsymbol{r}, t) = mn(\boldsymbol{r}, t)$, $n(\boldsymbol{r}, t) = \int d^3v f(\boldsymbol{r}, \boldsymbol{v}, t)$ is the number density and m is the mass of the microscopic particle. In the absence of external forces and when there are no interactions between the particles of the gas, as in point particles, the energy conservation law in a fixed frame is given by[5]

$$\frac{\partial \rho_E(\boldsymbol{r}, t)}{\partial t} = -\nabla \cdot \boldsymbol{J}_E(\boldsymbol{r}, t) \quad (3)$$

which when Eqs. (1) and (2) are substituted into will give

$$\int d^3v \left\{ \frac{\rho(\boldsymbol{r}, t)v^2}{2}\frac{\partial}{\partial t}\left[\frac{f(\boldsymbol{r}, \boldsymbol{v}, t)}{n(\boldsymbol{r}, t)}\right] + \frac{\rho(\boldsymbol{r}, t)v^2}{2}\boldsymbol{v}\cdot\nabla\left[\frac{f(\boldsymbol{r}, \boldsymbol{v}, t)}{n(\boldsymbol{r}, t)}\right]\right\}$$
$$+ \int d^3v \frac{f(\boldsymbol{r}, \boldsymbol{v}, t)}{n(\boldsymbol{r}, t)}\frac{\partial}{\partial t}\left[\frac{\rho(\boldsymbol{r}, t)v^2}{2}\right]$$
$$= -\int d^3v \frac{f(\boldsymbol{r}, \boldsymbol{v}, t)}{n(\boldsymbol{r}, t)}\nabla\cdot\left[\frac{\rho(\boldsymbol{r}, t)v^2\boldsymbol{v}}{2}\right] \quad (4)$$

The Liouville equation is given by[5]

$$\frac{\partial P^{(\bar{N})}}{\partial t} + \boldsymbol{V}\cdot\nabla P^{(\bar{N})} = 0 \quad (5)$$

where $\boldsymbol{V} = (\dot{\boldsymbol{r}}_1, \dot{\boldsymbol{r}}_2, \ldots, \dot{\boldsymbol{r}}_{\bar{N}}; \dot{\boldsymbol{p}}_1, \dot{\boldsymbol{p}}_2, \ldots, \dot{\boldsymbol{p}}_{\bar{N}})$ is the phase space velocity. Integrating Eq. (5) with respect to all of the phase space coordinates except the position $\boldsymbol{r}_1$ and the momentum $\boldsymbol{p}_1$ and assuming the absence of both pair potentials responsible for internal forces and the one particle potentials reponsible for external forces will give

$$\frac{\partial P^{(1)}}{\partial t} + \boldsymbol{V}\cdot\nabla P^{(1)} = 0 \quad (6)$$

where $P^{(1)} = P^{(1)}(\boldsymbol{r}_1, \boldsymbol{p}_1, t)$. But $P^{(1)} = f^{(1)}/\bar{N}$, with $f^{(1)}(\boldsymbol{r}, \boldsymbol{p}, t)$ being the generic distribution function.[6] The replacement of the distribution function in phase space by the distribution function in coordinate-velocity space in Eq. (6) will lead to

$$\frac{\partial}{\partial t}\left(\frac{f}{\bar{N}}\right) + \boldsymbol{v}\cdot\nabla\left(\frac{f}{\bar{N}}\right) = 0 \quad (7)$$

If one is to consider averaging over a finite volume element δV, then that would correspond to reducing the sample space over which the averaging is done. Moreover, δV can be chosen small enough such that $f(\boldsymbol{r}, \boldsymbol{v}, t)$ is constant over δV. Hence, Eq. (7) must be true only for the total number of particles in δV, in which case avoiding overcounting can be accomplished by dividing f by the total number of particles in δV only. The volume δV should be chosen such that it is a very large volume for molecular dimensions yet a very small volume for the macroscopic dimensions of the gas. Now $\bar{N} = \int_V d^3r \int d^3v f(\boldsymbol{r}, \boldsymbol{v}, t) = \int_V d^3r n(\boldsymbol{r}, t)$ is the total number of particles in the entire gas. Therefore,

Received 15 October 2002; revision received 2 December 2002; accepted for publication 6 December 2002.

*Assistant Professor, P.O. Box 5969, Department of Physics; alie@kuc01.kuniv.edu.kw.